CdS nanosheets as electrode materials for all pseudocapacitive asymmetric supercapacitors

VATTAKKOVAL NISHA[1], ANJALI PARAVANNOOR[1], DEEPTHI PANOTH[1],
SINDHU THALAPPAN MANIKKOTH[1], KUNNAMBETH M THULASI[1],
SHAJESH PALANTAVIDA[2] and BAIJU KIZHAKKEKILIKOODAYIL VIJAYAN[1],*

[1] Department of Chemistry/Nanoscience, Kannur University, Swami AnandaTheertha Campus, Payyannur 670307, India
[2] Centre for Nano and Materials Science, Jain University, Bangalore 562112, India
*Author for correspondence (baijuvijayan@gmail.com; baijuvijayan@kannuruniv.ac.in)

Abstract. Metal sulphides have recently been explored as a very promising pseudocapacitor electrode, owing to their unique physical, electronic and electrochemical properties. This study reports the synthesis and pseudocapacitor applications of 2D cadmium sulphide (CdS) nanosheets deposited on Ni foam via electrophoretic deposition method. Comprehensive morphological and electrochemical analyses were performed to elucidate the correlation between the structural features of CdS and their charge storage properties. The single electrode characterizations of CdS could exhibit a specific capacitance as high as 1165 F g^{-1} at 2 mV s^{-1}. An asymmetric supercapacitor prototype was also fabricated using the CdS nanosheets with ceria–titania nanotube composite (CeO_2–TNT) counter electrode. The device could exhibit an energy density as high as 14.58 Wh kg^{-1} at a power density of 1.9 kW kg^{-1}. At the end of 2000 cycles, the device could retain 100% of its initial capacitance.

Keywords. CdS nanosheets; electrophoretic deposition; pseudocapacitance; asymmetric supercapacitor.

1. Introduction

It is of great significance to build up ecofriendly and renewable energy sources and energy storage systems to beat the ever-increasing energy demand and the challenges associated with the use of fossil fuels [1]. Supercapacitors are one of the new generation energy storage systems that offer a very high power density and long cycling life. They are also considered as a green energy storage system, owing to their long cycling life, safe operation, environmental friendliness and capability to work in ample range of temperatures [2,3]. Supercapacitors have found their role in a range of applications like portable electronic devices, backup power supplies, load cranes, forklift, electric utilities and hybrid electric vehicles [4,5]. However, considering to replace or even complement batteries with supercapacitors possess a major challenge; i.e., their lower energy density. Therefore, efforts are under way to improve the energy density of supercapacitor systems by various means.

Generally, supercapacitors can be grouped into three categories based on their energy storage mechanism or cell configuration, i.e., electric double-layer capacitors (EDLCs), pseudocapacitors and hybrid supercapacitors. EDLCs store charge through electrostatic interaction at electrode–electrolyte interface. In EDLC's energy is stored non-Faradaically, and there is no charge transfer and redox reaction [6]. Unlike EDLC's, pseudocapacitors store charge through Faradaic process, which involves fast and reversible redox reactions between the electrode materials and electrolyte [7]. The specific capacitance and energy density of pseudocapacitors are generally found to be higher than EDLC's, as more charge can be stored both on surface and bulk of the electrode materials by electrochemical process and being a Faradaic system. Hybrid supercapacitors utilizes both the properties of EDLC and pseudocapacitors, in order to achieve higher power and energy density. On the basis of electrochemical configuration of supercapacitor device, supercapacitors can be also classified as symmetric and asymmetric. Symmetric supercapacitors are fabricated using identical electrodes, whereas asymmetric supercapacitors (ASc) are made of two different electrodes [8]. As we have two different electrodes in ASc, during charge–discharge process, we can take the benefit of two different potential windows of the electrodes in order to increase operating voltage of the full device [9]. Thus, an increase in operating voltage results in an increase in both energy density and capacitance value. Considering these facts, it would be beneficial to design an asymmetric pseudocapacitor system with appropriate choice of positive and negative electrodes to improve the storage and power

performances. Again, the conductivity values of the most widely used pseudocapacitor electrode systems are too low to support fast electron transport towards high rate capability and it is highly challenging to obtain a suitable material, which can overcome all these drawbacks.

Nanostructuring of individual electrode materials also helps in exhibiting better electrochemical performance by improving their energy density. Two-dimensional (2D) materials are now being widely used in this regard, as they offer several advantages that suit supercapacitor applications. These materials are single or few atom thickness layered ultra-thin crystals. They exhibit unique properties like higher surface area as they completely expose the surface atoms, i.e., no bulk volume, higher mechanical strength, transparency, flexibility and chemical stability. Moreover, in 2D nanosheets compared to basal planes, the edge sites are chemically more reactive and the electrolyte ions are intercalated through the Van der Waals opening [10,11]. While considering individual electrode materials, metal sulphides are being investigated as energy storage material with promising performance and also in a number of applications in the field of solar cell [12,13] and medical diagnostics [14] and supercapacitors [2,15,16]. They have high electrical conductivity and the best redox properties [17,18]. The metal sulphides show reversible redox reaction with alkaline electrolyte ($MS + OH^- \leftrightarrow MSOH + e^-$, where M is a transition metal). Among metal sulphides such as CdS, CuS, NiS, and CoS have shown substantial specific capacitance, notably due to the existence of valence states of materials that enhances the energy density of the device [19,20].

Cadmium sulphide (CdS) is considered as a desirable supercapacitor electrode material among the wide variety of metal sulphides. It has a narrow bandgap of 2.4 eV [21]. CdS semiconductors are identified as viable candidates for many different applications like supercapacitors, solar cells, light detectors, electrochemical biosensor and photocatalysis, owing to their good physical, electrical and optical properties [22]. CdS has been generally used in cadmium nickel batteries due to its long cycle life, high discharge rates, good environmental stability and high energy density. Some research groups have reported the application of CdS in various energy storage devices. Nair *et al* [3] have demonstrated CdS nanowire electrode with a specific capacitance of 181 F g^{-1} at a scan rate of 5mV s^{-1}. Ali *et al* [22] reported CdS/rGO/CeO$_2$ as electrode material with a specific capacitance of 407 F g^{-1} at 5 mV s^{-1}. Wang *et al* [23] have investigated the electrochemical performance of porous microsphere CdS on nickel foam, which exhibited a specific capacitance of 909 F g^{-1} at 2 mA cm^{-2}.

The unique porous nanosheet morphology of the CdS electrode material plays a vital role in the improved electrochemical performance. Porous nanostructures efficiently enhance the capacitance of supercapacitors, as they possess a high surface area with more electroactive sites, which facilitates the easy and fast diffusion of electrolyte ions into the interior portion of the electrode. The well-dispersed ultra-thin nanosheet structures also provide the effective access of electrolytes and layered nanosheets themselves act as mini-supercapacitor units connected in series or parallel. As far as we know, CdS nanostructures are less explored as electrode material for supercapacitor applications [24–27].

Thus, here in this study we mainly focus on the electrochemical performance of CdS as a supercapacitor electrode material. Besides that, CdS has a high theoretical specific capacitance value of 1675 F g^{-1}, which is also one of the reasons for considering CdS as the electrode material in this study [23]. The electrochemical performance of solvothermally synthesized CdS nanosheets coated on nickel foam via electrophoretic deposition (EPD) technique has been studied and investigated. The CdS nanosheets show a high specific capacitance of 1165 F g^{-1}. Moreover, an ASc was designed and fabricated by using CdS as the positive electrode and Ceria-deposited titanium nanotubes (CeO$_2$–TNT) as the negative electrode. CeO$_2$–TNT possesses excellent electrochemical properties with wide potential range and better cyclic stability. CeO$_2$–TNT was chosen as the negative electrode, in order to extend the potential window of the ASc and to overcome the limitations of both double layer capacitors (TNT) and pseudocapacitors (Ceria); redox pseudocapacitive ceria was deposited on the double layer capacitor TNT arrays [28].

2. Experimental

Cadmium chloride hemi (pentahydrate) (Merck, 81.0%), Sulphur powder (Merck, 99.5%), diethylene triamine (Merck, 98%), isopropyl alcohol (SRL, 99.5%), nickel nitrate (Merck, 98.5%), potassium hydroxide (Merck, 85%), commercial titanium metal sheet (Alfa Aesar, 99.5%), ammonium fluoride (SRL, 98%), ethylene glycol (SRL, 99%), cerous nitrate (Merck, 99.9%) and nickel foam were purchased and used as received without further purification.

2.1 *Synthesis of CdS nanosheets*

CdS nanosheets were prepared through solvothermal method. In a typical procedure, 0.1603 g of sulphur powder and 0.1827 g of cadmium chloride hemi (pentahydrate) (CdCl$_2$·2.5H$_2$O) were added to 30 ml of diethylenetriamine (DETA), in a 50 ml beaker and magnetically stirred for 1 h. After stirring, the solution was transferred to 50 ml Teflon-lined stainless steel autoclave. The autoclave was sealed and kept at 80°C for 48 h in a hot-air oven. Finally, the yellow precipitate of CdS was obtained. The resultant precipitate was washed several times with ethanol and water. Then dried inside a hot-air oven in air atmosphere at 70°C [29,30].

2.2 Fabrication of CdS electrode

EPD technique was used for the fabrication of the CdS electrode [24,31]. In a typical procedure, 10 mg of CdS powder and 0.8 mg of nickel nitrate were added to 20 ml of isopropyl alcohol in a beaker. The mixture was sonicated for 10 min to obtain a uniform dispersion. Nickel foam (2 cm × 2 cm × 0.2 mm) substrates were used as both positive and negative electrodes. Before using, it was washed with acetone and dilute hydrochloric acid (HCl), rinsed with deionized water and kept for drying in a vacuum oven. EPD was done at 50 V for 40 min to obtain a uniform CdS coating. After coating, Ni-foam was placed in a vacuum oven at 45°C for 24 h.

2.3 Fabrication of ceria-deposited TNT electrode

Modified single-step electrochemical anodization method was used for the preparation of titanium dioxide nanotubes. In anodization set up, platinum wire was used as the cathode and pure titanium foil as the anode. Pure commercial titanium metal sheet was cut into small rectangular shape. A quantity of 0.3 wt% ammonium fluoride solution in 100 ml ethylene glycol–water system containing 2 vol% water was used as electrolyte for anodization. Anodization was performed in an ice bath at 100 V for 1 h, while the electrolyte was continuously stirred using a magnetic stirrer. The foil was kept in ethanol for 15 min, dried and annealed at 400°C for 1 h in air. The prepared titania nanotubes (TNT) was dipped in a slanting position in 50 ml, 0.075 M cerium nitrate ($Ce(NO_3)_3$) aqueous solution for 1 h and dried under IR light for few minutes. After drying, it was annealed at 400°C for 1 h in air atmosphere to convert deposited cerous ions to ceria [28].

2.4 Fabrication of CdS//ceria-deposited TNT supercapacitor

An ASc was assembled using CdS as the positive electrode, ceria-deposited TNT as the negative electrode and 3 M KOH aqueous solution as the electrolyte. After assembling the CdS//ceria-deposited TNT supercapacitor, the coin cell was sealed using a manual crimper. The mass loading for positive electrode was 1.9 mg and that of negative electrode was 4.4 mg.

3. Characterization techniques

X-ray diffraction study was performed to identify the crystalline nature of the samples. Crystal structure of the synthesized CdS nanosheets were determined using X-ray diffractometer model D8 Advance (Bruker) with Cu Kα radiation (λ = 1.54178 A) at a scanning rate of 0.02° s^{-1} in the 2θ range from 20° to 80°. Morphological studies of the prepared nanostructures were analysed using scanning electron microscope (SEM) Hitachi SU8010 and transmission electron microscope (TEM) FEI TECNAI G2 Spirit BioTwin at different magnifications.

Electrochemical performances of the CdS nanosheets were studied using cyclic voltammetry (CV, BASi Epsilon), galvanostatic charge–discharge cycling (GCD, Neware Battery cycler) and electrochemical impedance spectroscopy (EIS, Bio-Logic) measurements. Electrochemical behaviour of the CdS nanosheets was analysed using a three-electrode system comprising of active material CdS nanosheets coated on nickel foam as working electrode, saturated Ag/AgCl as reference electrode, platinum as counter electrode and 3 M KOH as the aqueous alkaline electrolyte.

4. Result and discussions

4.1 Structural and morphological studies

The crystallinity of CdS nanosheet was characterized using XRD analysis. Figure 1a represents the XRD patterns of the as-synthesized CdS nanosheets. The diffraction peaks of CdS nanosheets at 2θ values 26.51, 28.18, 36.62, 43.68, 47.84, 51.80 can be indexed as the (002), (101), (102), (110), (103), (112) planes, corresponding to the Wurtzite structure of CdS (JCPDS:No. 65-3414). Figure 1b shows typical SEM micrographs of ultra-thin CdS nanosheets. SEM images reveal the surface morphology of the synthesized CdS to be 2D ultra-thin nanosheets. The sheet-like morphology plays an important role in the energy storing property due to its large surface area. Figure 1c and d displays the TEM micrographs of ultra-thin porous nanosheet morphology of CdS at different magnifications. The TEM images clearly demonstrate the well-dispersed, 2D ultra-thin nanosheets and it supports the morphology as provided in the SEM image.

### 4.2 Electrochemical properties of CdS electrode

The electrochemical performance of solvothermally synthesized CdS electrode was studied by using CV measurements in 3 M KOH electrolyte, using a standard calomel electrode (SCE) and platinum as the reference and counter electrode, respectively (figure 2a). Tests were carried out using CdS nanosheets at different scan rates 50, 30, 25, 20, 15, 10, 5 and 2 mV s^{-1} within a potential range of 0.08–0.6 V.

The curves show distinct cathodic–anodic peaks, revealing the pseudocapacitve behaviour of CdS in the KOH electrolyte, following the Faradaic reactions of the Cd^{2+}/Cd^{3+} redox couple.
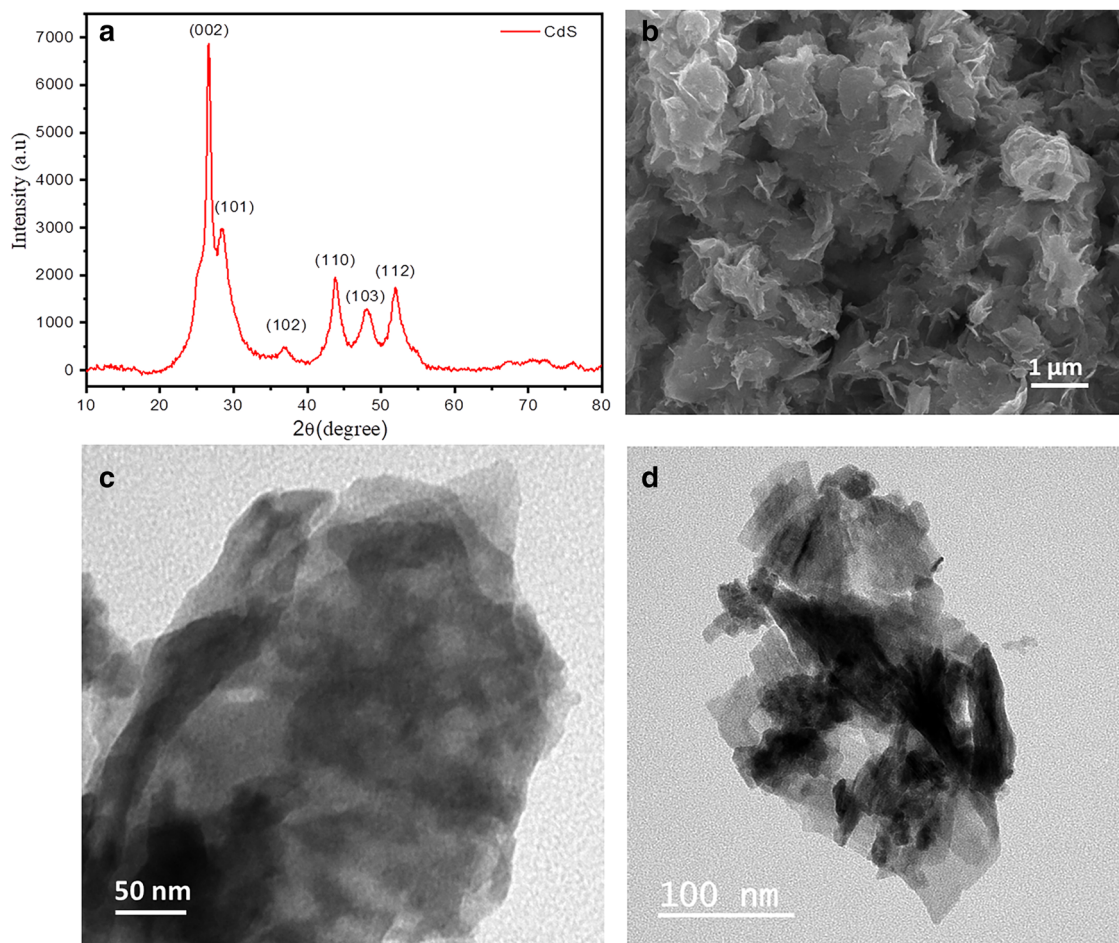
Figure 1. (**a**) XRD spectra and (**b**) SEM micrograph of CdS nanosheets. (**c** and **d**) TEM images of nanoporous CdS nanosheets at different magnifications.

The electrochemical reaction is shown below:

$$CdS + OH^- \leftrightarrow CdS(OH) + e^-$$
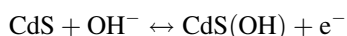
Specific capacitance is calculated by using the formula,

$$C = \int \frac{Idv}{2mv\Delta V} \tag{1}$$

The capacitance values were estimated using equation (1), where C is the capacitance, m the weight of the active material, v the scan rate and ΔV is the voltage window. The values obtained were 1165, 879, 675, 567, 488, 443, 393 and 250 F g^{-1} for the scan rates of 2, 5, 10, 15, 20, 25, 30 and 50 mV s^{-1}. The high specific capacitance values could be due to an amalgamation of several factors, including the binder-free EPD technique and the porous 2D structure of CdS sheets, enabling a better surface area and fast diffusion of ions. It is also evident from figure 2b that at lower scan rates the gravimetric capacitance increases. This means that the diffusion of OH$^-$ ions that are chiefly responsible for the redox behaviour has a direct relation with the CV scan rates. This correlation could be attributed to the fact that at lower scan rates, the entire electrode overlay including both the outer and the inner pore structures are effectively employed for OH$^-$ propagation. On the other hand, as the scan rates increases, interaction of the OH$^-$ could be restricted mainly at the outer regions owing to the lesser time for interaction, limiting the capacitance values [24]. The enhanced performance of the CdS electrode can be attributed to its continuous 2D porous nanosheet morphology, as it possesses an electrochemically active surface area favouring easy diffusion of the electrolyte ions.

The galvanostatic charge–discharge (GCD) test was conducted, so as to further assess the supercapacitor performance of CdS nanosheets. Figure 2c consists of GCD profiles of CdS electrode at different current densities 2, 5, 10, 15 and 20 A g^{-1} within the potential window 0–0.43 V. GCD curves of CdS electrode shows that, the discharge curves have the noticeable deviation of the shape from straight line again clarified that the capacitance is from Faradaic reactions and is not from electrostatic interaction at electrode–electrolyte interface. Each curve consists of a pair of charge plateau and discharge plateau located at 0.29–0.33 and 0.28–0.21, corresponding to the oxidation and reduction of Cd^{2+}. This behaviour is in good
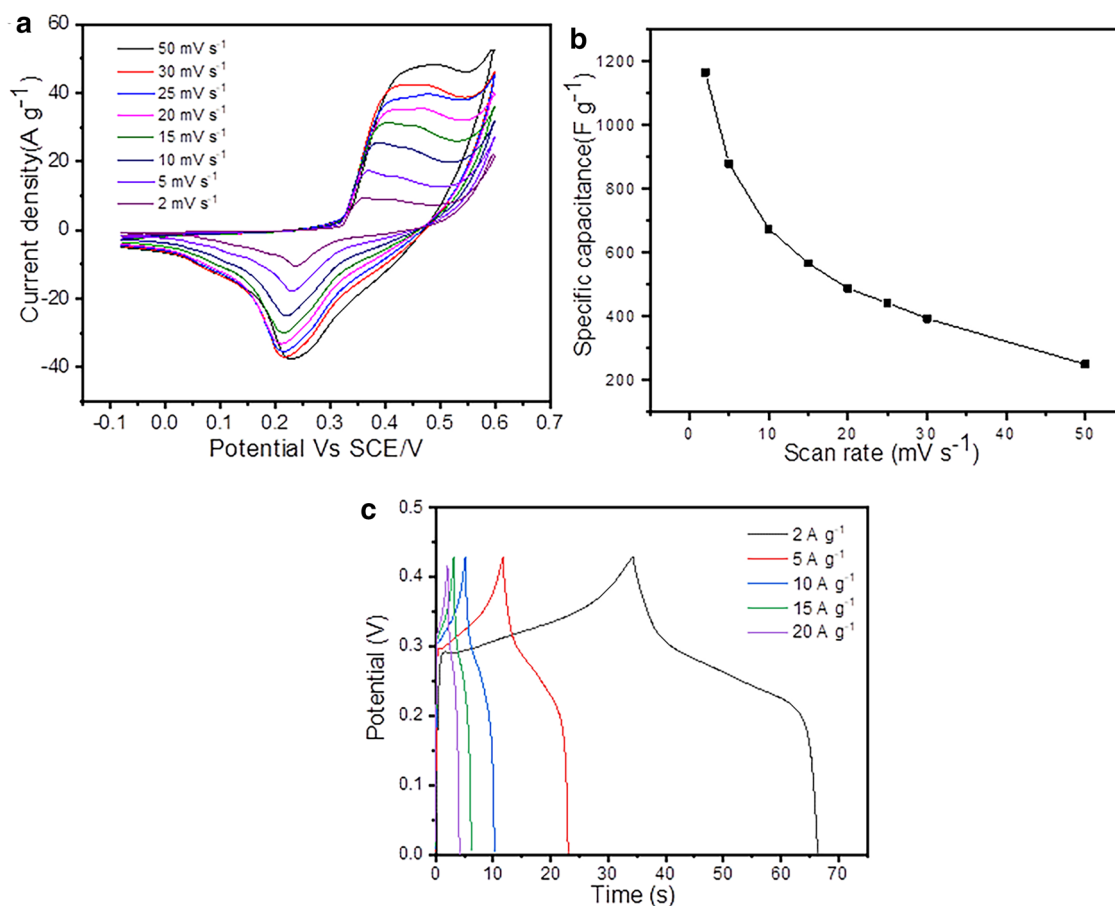
Figure 2. (a) CV curves of CdS nanosheets at different scan rates. (b) Specific capacitance *vs.* scan rate of the CdS nanosheets for CV curve. (c) GCD curves of CdS nanosheets at different current densities.

conformity with the pairs of redox peaks as shown in the CV curves.

The specific capacitance of electrode can be calculated from the following equation:

$$C_s = \frac{I\Delta t}{m\Delta V},\tag{2}$$

where C_s (F g^{-1}) is the specific capacitance, I (A) is the discharge current, Δt (s) is the discharge time, m (g) is the mass of electroactive material in the electrode, ΔV (V) the potential window. The calculated specific capacitance is 146, 131, 118, 105 and 90 F g^{-1} corresponding to the current densities of 2, 5, 10, 15 and 20 A g^{-1}, respectively.

4.3 *Electrochemical performance of CdS//CeO$_2$–TNT ASc*

The potential application of CdS nanosheet in a full-cell supercapacitor prototype was evaluated by fabricating an ASc using CdS nanosheets and CeO$_2$–TNT as the positive and negative electrodes, respectively. The electrochemical performance of the ASc CdS//CeO$_2$–TNT was investigated in the two-electrode measurements using 3 M KOH as the electrolyte. The following reactions are involved in fabricated ASc,

Cathode : CdS + OH$^-$ ↔ CdSOH + e$^-$

Anode : Ce^{IV}O$_2$ + K$^+$ + e$^-$ → Ce^{III}O$_2$K$^+$

The plots obtained from GCD analysis at different current densities (0.1, 0.2, 0.3, 0.4, 0.5, 0.75, 1 A g^{-1}) within the potential window of 0–1.95 V are shown in figure 3a. GCD plot shows a nonlinear relationship between the charge/discharge potentials and time. In addition, both charge and discharge curves retain the better symmetry, representing the excellent capacitance behaviour and electrochemical reversibility.

The specific capacitance (C_s), energy density (E), power density (P) were calculated from the GCD curves by using above equation (2).

$$E = \frac{CV^2}{2}\tag{3}$$

$$P = \frac{V^2}{4R}\tag{4}$$
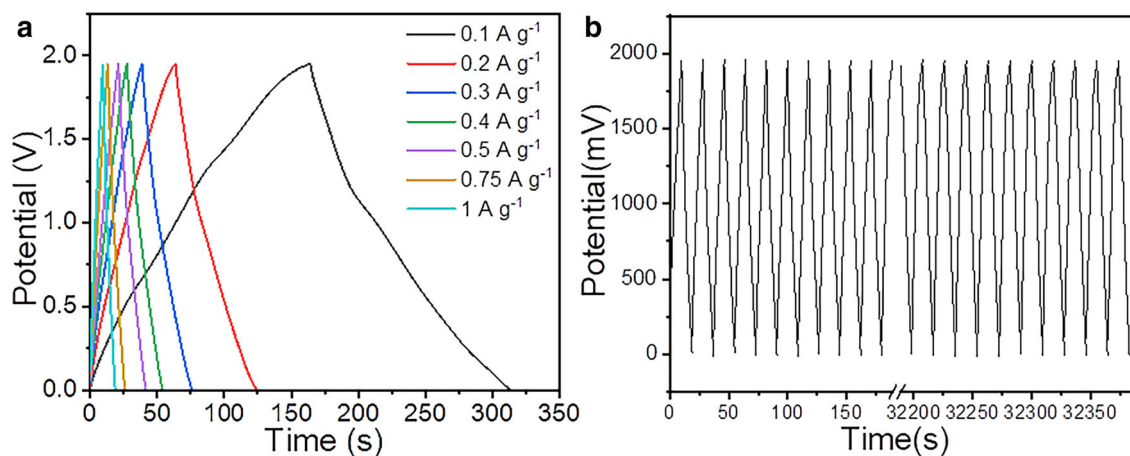
Figure 3. (a) GCD curves of CdS//CeO$_2$–TNT asymmetric supercapacitor at different current densities. (b) Cyclic stability of CdS//CeO$_2$–TNT asymmetric supercapacitor at a current density of 1 A g^{-1} by GCD measurement for 2000 cycles with 100% capacitance retention.

The fabricated ASc acquired a specific capacitance of 0.67 F g^{-1} at a current density of 0.1 A g^{-1}. Besides that, the assembled capacitor can deliver a high energy of 14.58 Wh kg^{-1} with power density of 1.9 kW kg^{-1} at the potential 1.95 V [32]. The superior energy performance could be due to the higher capacitance as well as voltage window as compared to other full-cell devices based on alkaline aqueous electrolytes, owing to the careful selection of positive and negative electrodes.

The cycling performances of CdS//CeO$_2$–TNT ASc were evaluated over 2000 cycles, carried out at a current density of 1 A g^{-1}, as shown in figure 3b. At the end of 2000 cycles, the capacitance retention was found to be 100%, which indicates the long-term electrochemical stability in KOH electrolyte, in agreement with the results obtained from EIS spectra [33,34].

The better cyclic stability could be due to different factors, including the 2D nature of CdS ensuring a continuous and stable ion intercalation and deintercalation, better reaction kinetics and better conductivity even in the absence of a conducting additive. The binder-free approach in the case of both electrodes could also be a contributing factor in improving the conductivity and cyclic stability of the device.

EIS analyses were performed to further analyse the device prototypes. Figure 4 shows the EIS of cell, before and after charge/discharge cycling, measured with 3 M KOH solution at frequencies ranging from 100000 to 0.01 Hz. The Nyquist plots consist of a semicircle at high frequency region and a linear part at low frequency region. The linear part in the low frequency region, representing the Warburg impedance (W), indicates the rapid ion diffusion both in the electrolyte and on the surface of the electrodes corresponding to the ideal capacitive behaviour of the electrodes. The diameter of the semicircle indicates the charge-transfer resistance (R_{ct}) offered by redox reactions at the electrode–electrolyte interface. The calculated R_{ct} for uncycled sample is 6.12 Ω. At the end of 2000 cycles, the
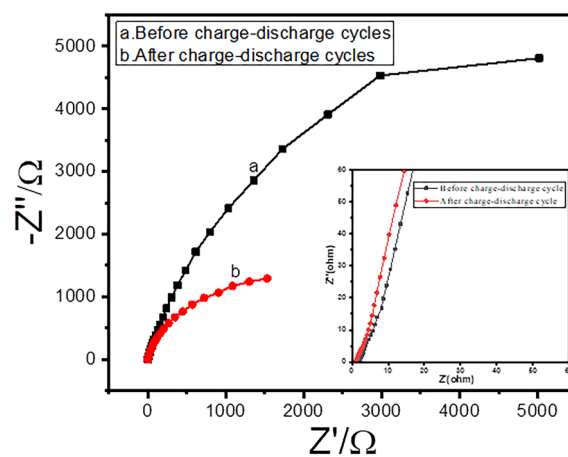
Figure 4. Electrochemical impedance spectra of CdS nanosheets before and after charge–cycles and inset shows the enlarge region in the high frequency.

R_{ct} was reduced to 5.05 Ω. At high frequencies in the Nyquist plots, the intercept at the X-axis (Z') indicates the equivalent series resistance, which is the sum of inherent resistance of the active material, the bulk resistance of electrolyte and the contact resistance at electrode–electrolyte interfaces [24,35]. The series resistance is 1.6 Ω before cycling and after cycling, it was diminished to 0.9 Ω. The EIS results indicate a lower charge transfer resistance and ion diffusion resistance with fast reaction kinetics. The results are in line with the cycling data, which shows 100% capacitance retention.

5.   Conclusion

In conclusion, solvothermally synthesized CdS nanosheets coated on nickel foam by EPD method was found to be a promising candidate for superior pseudocapacitor

electrodes. The 2D structure of CdS nanosheets along with the binder-free electrode fabrication technique enables better electrochemical performance, high specific capacitance of 1165 F g^{-1}, and good rate capability. Moreover, we have fabricated an ASc by using CdS nanosheets as the positive electrode, and CeO$_2$–TNT as the negative electrode and 3 M KOH aqueous solution as electrolyte. This ASc device gives energy density as high as 14.58 Wh kg^{-1} at a power density of 1.9 kW kg^{-1}, within the potential range 0 to 1.95 V and good cyclic stability at the end of 2000 cycles. These hopeful studies display the potential value of CdS as an efficient supercapacitor electrode material.

Acknowledgements

References

[1] Bhise S C, Awale D V, Vadiyar M M, Patil S K, Ghorpade U V, Kokare B N *et al* 2019 *Bull. Mater. Sci.* **42** 1

[2] Zhu T, Xia B, Zhou L, Wen D and Lou X 2012 *J. Mater. Chem.* **22** 7851

[3] Nair N, Majumder S and Sankapal B R 2016 *Chem. Phys. Lett.* **659** 105

[4] Bao S J, Li C M, Guo C X and Qiao Y 2008 *J. Power Sources* **180** 676

[5] Wang J, Polleux J, Lim J and Dunn B 2007 *J. Phys. Chem. C* **111** 14925

[6] Libich J, Máca J, Vondrák J, Čech O and Sedlaříková M 2018 *J. Energy Storage* **17** 224

[7] Xu B, Pan L and Zhu Q 2016 *J. Mater. Eng. Perform.* **25** 1117

[8] González A, Goikolea E, Barrena J A and Mysyk R 2016 *Renew. Sustain. Energy Rev.* **58** 1189

[9] Shao Y, El-Kady M F, Sun J, Li Y, Zhang Q, Zhu M *et al* 2018 *Chem. Rev.* **118** 9233

[10] Kumar K S, Choudhary N, Jung Y and Thomas J 2018 *ACS Energy Lett.* **3** 482

[11] Yu Z, Tetard L, Zhai L and Thomas J 2015 *Energy Environ. Sci.* **8** 702

[12] Kung C W, Chen H W, Lin C Y, Huang K C, Vittal R and Ho K C 2012 *ACS Nano* **6** 7016

[13] Gur I 2005 *Science* **310** 462

[14] Rui X, Tan H and Yan Q 2014 *Nanoscale* **6** 9889

[15] Han S C, Kim H S, Song M S, Lee P S, Lee J Y and Ahn H J 2003 *J. Alloys Compd.* **349** 290

[16] Lai C H, Huang K W, Cheng J H, Lee C Y, Lee W F, Huang C T *et al* 2009 *J. Mater. Chem.* **19** 7277

[17] Chan W C 1998 *Science* **281** 2016

[18] Hou L, Yuan C, Li D, Yang L, Shen L F, Zhang F *et al* 2011 *Electrochim. Acta* **56** 7454

[19] Nair N and Sankapal B R 2016 *New J. Chem.* **40** 10144

[20] Xia H, Feng J, Wang H, Lia M O and Lu L 2010 *J. Power Sources* **195** 4410

[21] Adhikari A De, Oraon R, Tiwari S K, Saren P, Lee J H *et al* 2018 *Ind. Eng. Chem. Res.* **57** 1350

[22] Ali A A, Nazeer A A, Madkour M, Bumajda A and Al Sagheer F 2018 *Arab. J. Chem.* **11** 692

[23] Wang X, Shi B, Fang Y, Rong F, Huang F, Que R *et al* 2017 *J. Mater. Chem. A* **5** 7165

[24] Xu P, Liu J, Yan P, Yin Y, Miao C, Ye K *et al* 2016 *J. Mater. Chem. A* **4** 4920

[25] Chang B, Zhang S, Sun L, Yin H and Yang B 2016 *RSC Adv.* **6** 71360

[26] Choi M, Na K, Kim J, Sakamoto Y, Terasaki O and Ryoo R 2009 *Nature* **461** 246

[27] Liu J and Wei L X 2012 *Adv. Mater.* **24** 4097

[28] Thulasi K M, Manikkoth S T, Paravannoor A, Palantavida S, Bhagiyalakshmi M and Vijayan B K 2019 *J. Phys. Chem. Solids* **135** 109111

[29] Xu Y, Zhao W, Xu R, Shi Y and Zhang B 2013 *Chem. Comm.* **49** 9803

[30] Ma S, Xie J, Wen J, He K, Li X, Liu W *et al* 2017 *Appl. Surf. Sci.* **391** 580

[31] Chavez-Valdez A, Shaffer M S P and Boccaccini A R 2013 *J. Phys. Chem. B* **117** 1502

[32] Tang P, Zhao Y, Xu C and Ni K 2013 *J. Solid State Electrochem.* **17** 1701

[33] Shanmugavani A and Selvan R K 2016 *Electrochim. Acta* **188** 852

[34] Surendran S, Shanmugapriya S, Shanmugam S, Vasylechko L and Selvan R K 2018 *ACS Appl. Energy Mater.* **1** 78

[35] Joji Reddy B, Vickraman P and Simon Justin A 2019 *Bull. Mater. Sci.* **42** 1